Review of Scientific Instruments

Ion beam intensity and phase space measurement techniques for ion sources

Cite as: Rev. Sci. Instrum. **93**, 011501 (2022); https://doi.org/10.1063/5.0075110
Submitted: 13 October 2021 • Accepted: 15 December 2021 • Published Online: 24 January 2022

T. Kalvas

Review of Scientific Instruments REVIEW scitation.org/journal/rsi

Ion beam intensity and phase space measurement techniques for ion sources

Cite as: Rev. Sci. Instrum. 93, 011501 (2022); doi: 10.1063/5.0075110
Submitted: 13 October 2021 • Accepted: 15 December 2021 •
Published Online: 24 January 2022

T. Kalvas[a)]

AFFILIATIONS

Department of Physics, University of Jyväskylä, P.O. Box 35 (YFL), 40014 Jyväskylä, Finland

Note: This paper is a part of the Special Topic Collection on Ion Source Diagnostics.
[a)]**Author to whom correspondence should be addressed:** taneli.kalvas@jyu.fi

ABSTRACT

Ion sources produce beams used in accelerators and other applications. Both development and use of ion sources need beam diagnostics to probe the plasma processes and beam formation for optimization purposes and to produce beam parameters needed for transport tuning. These diagnostics include beam intensity measurements usually carried out with Faraday cups or inductive pickups, magnetic separation, profile measurements with scintillation screens and wires, and phase space measurements with different types of emittance scanners.

I. INTRODUCTION

The basic purpose of an ion source is to produce a beam of charged atoms or molecules. Therefore, perhaps the most fundamental diagnostic to be carried out on an ion source is the measurement of the ion beam intensity, usually indicated as current or a rate of charges, being extracted from the source. In the simplest case, the measurement can be carried out directly by having the beam collide with a Faraday cup (FC), a conductor grounded through an ammeter recording the flow of charges. Other more advanced techniques for beam intensity measurement are also widely in use, such as particle counting, inductive measurement, and calorimetry. The beam intensity measurement is, of course, important in itself, providing a probe for characterizing the beam production and transport efficiency, but it also forms a basis for many other diagnostics when combined with spatial selectivity and electrostatic and magnetic bending. These include the standard tools of the trade: species separation, profile measurement, and phase space diagnostics. Many of these methods are commonly in use also at higher energies, and therefore, they are extensively covered in multiple materials.[1,2] Therefore, in the following chapters, these different techniques for ion beam based diagnostics are reviewed, especially considering their use under ion source relevant conditions.

II. BEAM INTENSITY MEASUREMENT

A. The Faraday cup

A Faraday cup is an instrument for determining the instantaneous current of the beam of charged particles. It works by stopping the beam in an insulated conductor and measuring the rate of charges flowing to the ground through an ammeter. The principle of operation is very simple, but the accuracy of such measurement can be compromised by emission of secondary electrons, backscattering of measured ions or their electrons, ghost signals due to stray beams, and unidealities of the ammeter electronics.

The emission of secondary electrons (SEs) is the main source of error in the typical ion source FC diagnostic. The electrons may be emitted due to transfer of potential energy (potential emission) and/or kinetic energy (kinetic emission) between the incoming ion and the FC atoms and electrons.[3] The potential emission is related to electronic transitions and an Auger-type process before impact and is most abundant at energies $\lesssim 10$ keV/u.[3] At higher energies, the kinetic emission, on the other hand, takes place within the FC material by transferring enough kinetic energy to material electrons to enable backscattering, transmission to the surface, and emission into vacuum. As the process takes place close to the surface, the SE yield Y_{se}, the number of emitted electrons divided by the number incoming ions, is roughly proportional to the surface electronic stopping power of the projectile in the FC material.[4] For protons, Y_{se} peaks at 100 keV, having a maximum of 1.7 for a copper target, which goes down to 0.7 at 10 keV and at 1 MeV.[5] In many ion source relevant cases, the energy of the incoming ion is ~10 keV/u, where the potential emission and kinetic emission processes are interrelated, and thus, the SE emission physics become quite complex, especially for heavy ions. This can lead to Y_{se} ranging from 0.1 for singly charged ions to 100 for very high charge state heavy ions.[6,7] The yield is also dependent on surface purity and oxidation, making its

prediction challenging under experimental conditions.[8] Regardless of the incoming ion species, energy, and target material, the energy distribution of the emitted electrons is peaked at a few eV with an FWHM of the same magnitude. This main peak typically contains about 90% of the emitted electrons, and their angular distribution has a cosine shape with respect to the surface normal. The rest of the SEs follow decaying exponential-like curves in energy and are a result of more direct kinetic energy transfer from the incident ion to the electrons. As such, the highest energy electrons are also emitted mostly in the forward direction and are therefore emphasized especially in the case of incident angles far from the surface normal.[5] Nevertheless, the distribution also contains some backscattered high energy electrons, making capturing of all the SEs challenging.

The standard solution for capturing the emitted SEs within the FC and therefore avoiding the alteration of the measured ion beam current signal is a so-called electron suppression electrode biased at some tens or hundreds of volts of negative potential with respect to the cup. Such construction produces an electric field, which pushes the relatively low-energy electrons back to the FC. An example of such a design is shown as a simulation plot, also presenting the incoming ion beam, the suppressing field, and the SEs, in Fig. 1. The simulation, made with IBSimu,[9] models the SEs with a typical semi-empirical model,[10] reproducing the main features of the distribution. As such, the simulation is capable of predicting the effect of the cup geometry, the electron suppression electrode voltage, and the charge distribution on the suppression efficiency, which is >90%

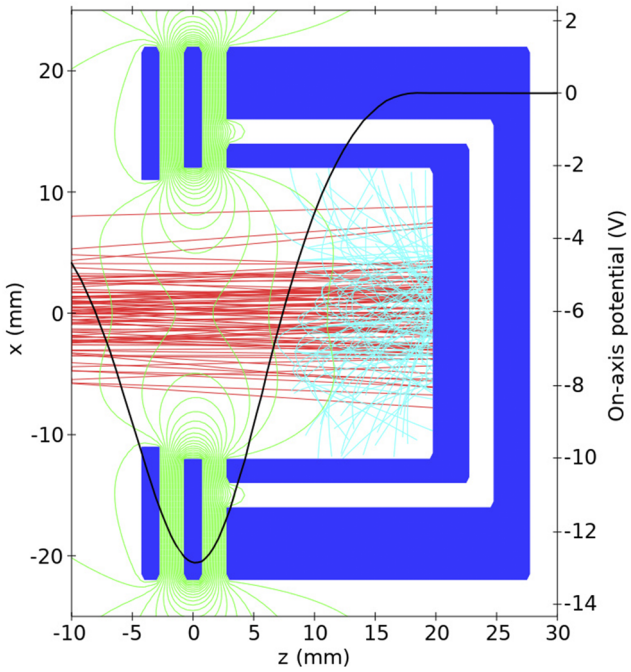

FIG. 1. Faraday cup simulation plot with incoming 80 keV, 100 μA Ar^{8+} beams (red), secondary electrons (cyan), electrodes (blue), and equipotential lines (green). The electron suppression electrode (at $z = 0$ mm) is on −100 V potential, and the rest of the electrodes (collimator at $z = -4$ mm and FC and its shield at $z > 3$) are on 0 V. The on-axis potential is overlaid with a black curve.

for the presented case with incoming 80 keV, 100 μA Ar^{8+} parallel beams with a 2.5 mm rms radius and −100 V suppression voltage. The efficiency drops with increasing beam potential as the beam potential modifies the suppression potential barrier. As an example, with the presented 100 μA incoming beam, the barrier has a minimum of −13 V on-axis; with a 100 nA beam, the barrier is −17 V, and with a 200 μA beam, it is only −9 V if all other parameters are kept constant. It is therefore obvious that the presented FC should only be used with low beam currents. In practice, the electron suppression can be tested by sweeping the suppression voltage and verifying that the observed beam current saturates at high suppression voltages. The electron suppression of the FC also performs another function as it blocks the low-energy electrons trapped within the positive ion beam potential from entering the cup and affecting the measurement. On the other hand, the typically low suppression voltages that are not capable of blocking the higher energy SEs emitted in the forward angles of the grazing angle have an impact on the FC collimator plate, a separate collimating device upstream of the FC or on the beam pipe. Such electrons may therefore affect the FC reading, but fortunately, they are not very abundant at ion source relevant energies.

An alternative way of implementing the suppression is by using a magnetic field to prevent the SEs from escaping. By integrating SmCo permanent magnets in a compact FC, a 50 mT flux density can be produced. With such a field, the ~10 eV secondary electrons have a gyroradius of 0.2 mm, trapping them within the FC. The drawback in using permanent magnets is that the temperature of the structure housing the magnets has to be well controlled to avoid demagnetization. Nevertheless, in most ion source related cases, FCs require water cooling or use of a specifically engineered path for the heat to be conducted out of vacuum. In such cases, the electric isolation of the FC from the ground needs to be made without obstructing the heat conduction. Methods include the use of high-heat-conductance ceramic isolators (AlN and BeO), use of low-conductance water as an electric isolator, and use of insulating vacuum breaks, and the choice depends on the beam intensity range of the FC in question.

The beam intensities, which are usually measured with FCs in ion source relevant energies, range from 1 A down to about 1 pA. In the high-current end of the range, the applicability of the technique is limited by the power handling capability of the collector and can reach an average of tens of kW if directly water-cooled. The low currents, down to 1 pA, can be reached with careful mechanical and electrical design, avoiding noise sources and leakage where possible.[11] For example, the use of triaxial cabling to avoid microphonics and electrical noise is absolutely necessary in a typical accelerator laboratory setting. The choice of measurement electronics is also crucial, and usually, technologies based on the picoammeter or switched integrator transimpedance circuits are used. At the lowest intensities, the fundamental noise sources, such as the shot noise, are unavoidable and are therefore only limited by the measurement bandwidth.

While the measurement bandwidth for most beam current measurements is limited by the measurement electronics, in the most time-critical applications, such as time-of-flight (TOF) measurement, the whole measurement system should be impedance matched. Impedance matching avoids formation of reflections in the FC signal chain, which would cause difficulties in interpreting fast signals. Typically, such a system is matched to 50 Ω, starting

from the cylindrical geometry, with the FC collector and the shield forming a coaxial transport line, which is then connected to a 50 Ω coaxial vacuum feedthrough and in the end connected to impedance matched measurement electronics.[12]

B. Non-destructive methods

Even though FCs are simple and robust, it is sometimes beneficial to measure beam current without disturbing the beam propagation. This is the case especially for operational ion sources where the beam is being delivered to the accelerator, and for on-line tuning of the source, measurement of the beam current would be needed. In most cases, the total current flowing from the ion source can be measured from the ion source high voltage bias supply. Unfortunately, in many cases, this reading is not a good indication of the ion beam current intensity. The beam current might be collimated in the extraction, and the bias current may also include other components such as backstreaming electrons or leakage currents due to the source water cooling. The beam current of interest might as well be only a part of the total beam extracted from the source as is the case with the Electron Cyclotron Resonance Ion Source (ECRIS), which always tends to produce a distribution of charge states.[13] Therefore, methods capable of measuring a propagating ion beam in a non-destructive manner are often of interest.

The operation principle of non-destructive beam current measurement is to take advantage of the electromagnetic field induced by the beam, i.e., by measuring either the magnetic or the electric field with capacitive or inductive pickups.[14] Capacitive pickups are usually only used at high energies, but inductive measurement is useful also at low energies even though most units described in the literature were developed for high energy accelerators. When measuring a pulsed ion beam, the beam current transformer (BCT), which acts as a classical transformer, can be used. The toroidal transformer core is placed around the beam pipe, with an isolating gap stopping the wall currents. The pulsed beam current produces a varying magnetic flux in the transformer core, which induces a voltage on the secondary wound around the same core producing the output signal. Such a passive BCT suffers from rather high low-frequency cutoff, causing a signal droop, which is why most BCTs are of an active type with an additional feedback winding. The active feedback circuit shown in Fig. 2 decreases the cutoff-frequency by the amplification factor A of the operational amplifier used and provides a very good beam

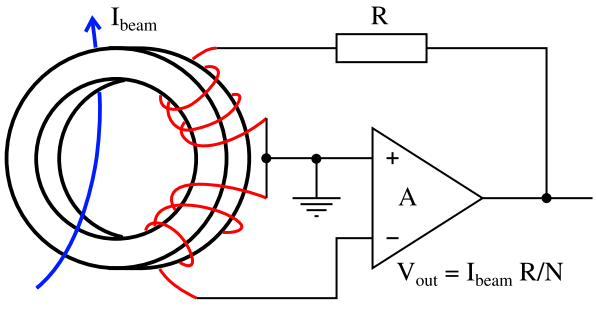

FIG. 2. Active feedback beam current transformer.

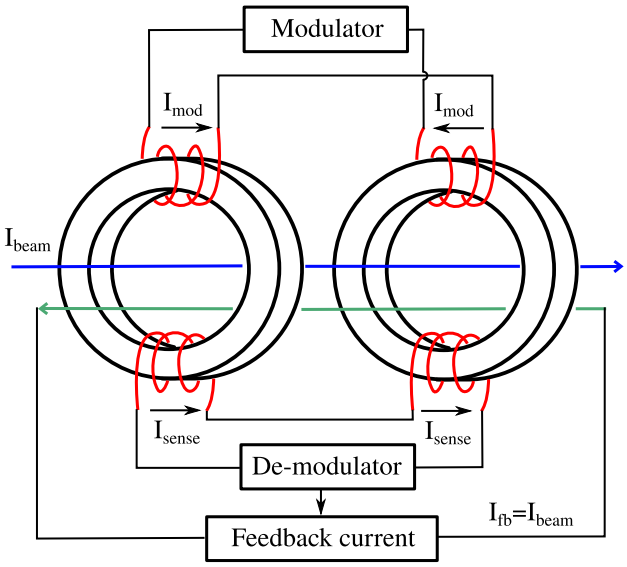

FIG. 3. DC current transformer.

pulse shape representation on the output.[15] These devices have typical bandwidths from 1 Hz to 1 MHz and sensitivities in the μA level.

With continuous beams, induction on the secondary does not take place as the beam magnetic field is constant. Nevertheless, inductive measurement of a DC beam current is possible with a device known as the direct current transformer (DCCT).[16] The DCCT operates by exciting the transformer cores with a modulator circuit, which drives the cores to saturation in positive and negative directions (see Fig. 3). The beam current causes an imbalance in the saturation visible on the secondary windings, which is used to drive a feedback current through the cores to nullify the imbalance. The feedback current then reproduces the beam current with a sensitivity of about 1 μA and a bandwidth starting from DC and going up to some kHz. Modern DC transformers such as the parametric current transformer combine the modulator circuit with the active pulse transformer to provide a wider bandwidth response.[17]

C. Particle multipliers

While beam currents down to the pA level can be measured with an FC and an ammeter, it can be beneficial to be able to measure even lower intensities even though such beams are not usually of interest for beam production. They can, however, be useful for diagnostic purposes, especially when combined with spectrometry or other scanning methods that limit the beam intensity. The measurement of the lowest beam intensities is usually achieved by a particle multiplier or a two dimensional multichannel plate (MCP).[18] In both of these devices, the primary ion produces secondary electrons in a collision with an electrode, which then in subsequent collisions generate a cascade of secondary electrons, effectively multiplying a single charge by a factor of 10^6 or more. The final charge can then be collected on an anode and read using an ammeter, or especially in the case of an MCP, it can collide with a scintillating screen, producing visible light representing the original particle distribution. While

these devices can be used in a continuous mode measuring the output current, which is proportional to the incoming beam current, the highest sensitivity is achieved by measuring single particles and by making the intensity measurement using a pulse counter. Such a measurement requires a very high gain and a sufficient incoming particle energy to ensure generation of the electron cascade at every particle. While such a measurement provides a very high sensitivity, it is not capable of measuring particle fluxes of more than 10^6 particles/s.

III. BEAM SPECTROMETRY

While beam intensity measurement is of interest on its own, in many cases, the diagnostic possibilities broaden when it is combined with magnetic and electrostatic bending or timing of particle propagation for ion beam spectrometric purposes. In a typical ion source application, the beam energy is mostly determined by the source potential U relative to the beamline. If one assumes the kinetic energy of charged particles is zero at U, the magnetic rigidity $B\rho = p/q$, where B is the magnetic field, ρ is the bending radius, p is the particle momentum, and q is the particle charge, takes the form $B\rho = \sqrt{2mU/q}$ in the classical limit. The magnetic field, typically in a form of magnetic dipole, is capable of separating particles extracted from the source by their differing m/q values. Such separation is routinely used, for example, in the negative ion plasma sources to separate the ions of interest from the co-extracted electrons using permanent magnets.[19] The electrons are usually dumped within a cavity in an electrode, and the escape of secondary electrons is suppressed by the dumping magnetic field itself. The control of the secondaries is first important to avoid problems caused by charging of extraction insulators and heating of electrodes and to provide a meaningful diagnostic of the intensity of the co-extracted electron beam. In some negative ion sources, electron dumping is made immediately after the plasma electrode, with electrons ending up between the plasma and puller electrodes.[20,21] In these cases, it is quite possible that the current measured on the puller electrode does not represent the fully extracted electron beam intensity as a part of the electrons may end up on the plasma electrode.

Another application where magnetic separation is routinely used is with ECR ion sources, in which the ion beam of interest with selected mass and charge is separated from all other particle species. In typical systems, a mass resolving power in the range of 1/100 is sufficient and can be achieved with dipole magnets with a bending radius of about 500 mm. The separation of particle species is, of course, important not only for beam production using the ECRIS but also as a tool for diagnostics as it enables probing the plasma with charge state distribution (CSD) measurements and by making other diagnostics such as profile and emittance measurements and energy analysis on the separated species.[22] On typical CSD separation application on the ECRIS, it is critical that the FC is well shielded on all sides and therefore only measures the beam entering through the front collimator. Otherwise, it is very easy to produce negative side peaks on the spectrum due to secondary electrons produced in collision with the vacuum chamber walls. The magnetic separation can also be used for other types of spectrometry as the magnetic rigidity is a function of particle momentum. As an example, in Ref. 23, Izotov *et al.* used a magnetic dipole and an electron multiplier for measuring the energy distribution of electrons escaping the magnetic bottle of an ECR ion source, providing a unique probe for the electron energy distribution in the plasma. In some extreme cases, the magnetic separation does not provide a sufficient resolution. In these cases, it may be possible to use a cyclotron to separate species with close m/q values. By combining such separation with particle counting, it is possible to separate and evaluate the production of extremely high charge states and elements produced from plasma chamber sputtering, which may be used for plasma diagnostics and also for beam production in cases where only minute intensities are required.[24]

Electrostatic field alone does not separate particles as in a purely electrostatic system, the particle trajectories are not dependent on the particle mass or charge. By using an electrostatic field E_x perpendicular to magnetic field B_y, with both being perpendicular to the beam velocity v_z, and observing the particles not bending in the combined field, one can produce a so-called Wien filter.[25] Particles not bent have Lorentz force $F = q(E_x - v_z B_y) = 0$, making the filter a velocity selector, where $v_z = E_x/By = \sqrt{2qU/m}$. Similar to the magnetic separator, the Wien filter separates particles by m/q. For example, in Ref. 26, a compact Wien filter was used to separate the hydrogen species and impurities produced by a 2.45 GHz microwave ion source. Another possibility for separating particle species emitted by an ion source in a compact setting is to use time-of-flight analysis.[27] Such a system requires a method for fast chopping to produce the beam pulse to be measured. A fast beam intensity measurement placed at a distance L from the pulser is used to produce a TOF spectrum, where flight time is inversely proportional to the ion velocity $t = L/v$. Naturally, such analysis suits pulsed ion sources well, but in many cases, the time to reach stable plasma conditions and beam formation is not fast enough to allow TOF analysis at high resolution. Therefore, additional pulsing with high voltage electrodes acting on the beam is usually required.

IV. BEAM PROFILES

The knowledge of the transverse distribution of the beam is one of the basic diagnostics and is essential for almost any ion source or LEBT setup. The distribution gives essential information on the beam formation, possible losses, and aberrations in the extraction and aids in tuning the beam for further transport. The easiest and most direct way of determining the beam profile is to use a scintillation screen. The screen is exposed to the beam usually in a 45° angle, and the scintillation light is observed with a CCD camera though a viewport in a transverse direction. The measurement directly gives the two-dimensional beam distribution. Several scintillation materials are commercially available, and many of them are well characterized for use with high energy ion beams. Nevertheless, many of these materials are also beneficial at ion source relevant energies.[28,29] The main disadvantages of the method are aging of the screens[30] and saturation at high intensities. In addition, close to the ion source, visible light emission from plasma may interfere with the imaging. At high intensities, where scintillation screens are typically not used, it is possible to carry out 2D profiling of ion beams by calorimetry. The hardware can be as simple as a metal sheet heated by the beam and cooled mainly by radiation, which is then imaged with an infrared (IR) camera.[31] The calculation of the beam profile

from such an image is unfortunately challenging due to heat conductance within the sheet. The analysis can be simplified and the spatial resolution can be improved by using a pixelized target. Such profilometry is commonly used with ion sources for fusion and may also be equipped with thermocouples and water calorimetry for better absolute beam intensity accuracy.[32] Nevertheless, none of the 2D profile measurement methods can compete with the accuracy and convenience of direct current measurements of an FC with secondary electron suppression. One option to gain spatial resolution is to have the FC collector segmented within a common cup body[33] or to have an array of completely separated FCs in one structure.[34] Wiring of such devices can become quite messy if compact high pixel density 2D profiles are required. One option for such a device could be a row of FCs in the x-direction and scanning with a stepper motor in the y-direction.

Traditional alternatives for 1D beam profile measurement include scanning wires or harps and grids. In these devices, the beam is intercepted by one or multiple thin wires, usually with diameters from 10 μm to some hundreds of μm. The wire-to-wire distance is much greater, making the method almost non-destructive. The beam particles at ion source relevant energies are stopped within the wire, depositing their charge within, and similar to FCs, the associated secondary electrons are emitted. The beam profile in one transverse direction is reproduced from the current measured on the wire, which is proportional to the ion beam density. Often the diagnostic system contains separate or integrated wires in a single motion feedthrough for profiling in both x and y directions. A two-dimensional model of the beam profile can be numerically reconstructed with limitations using Abel inversion. In high energy positive ion accelerators where the beam particles are not stopped within the wire, the measured signal of interest is produced only by the secondary electrons. Hence, these devices are often known as secondary electron monitors (SEMs). With positive ion beams at low energies, the signal is simply a sum of the ion beam current and the SEs as the electrons are accelerated away from the wire by the beam potential, making the measured intensity proportional to the intercepted beam. With negative ion beams, the SEs may be partially suppressed by the beam potential depending on the beam intensity and diameter. In such a case, a high quality signal can be produced by using a separate SE suppression frame with a high voltage to reach full suppression.[35] The advantage of using wires as opposed to scintillation screens for profile measurement is that the wires provide a linear response to beam intensity over many orders of magnitude. In the low-intensity end, the measurement is limited by noise, typically at some pA/wire level. At the high end, the limitation arises from beam power. The cooling of a thin measurement wire is dominated by radiation, and the peak temperatures are typically high. The choice of wire material (usually refractory metals or carbon), thickness, and the possible wire scanning speed should be made taking into account the beam energy density and time structure to not only avoid the melting point but also the thermionic emission, which again would have an effect on the intensity measurement.[36] An alternative method for wire scanners is to use an optical fiber instead of a metallic wire. Scintillation light produced in a possibly doped fiber can be led long distances to a noise-free environment for detection. Using single photon counting, a measurement with a sensitivity of <1 pA has been demonstrated.[37] Higher beam currents can be detected simply with photodiodes. The optical fiber cannot withstand high power densities as metal wires, which limits the method to low power beams. A modern, non-destructive alternative for acquiring a 1D beam profile is to use injected gas or even residual gas to produce light via ionization or excitation to image the particle distribution.[38] The method is readily available with minimal need for hardware. Only a vacuum window is needed on the beam pipe and a large sensor digital camera with a capability for long exposures.

In many cases, the goal of the profile measurement is to provide a result, which somehow quantifies the size of the beam. One of the most often used beam parameters describing the beam size is the rms (root mean square) size, i.e., the standard deviation of the beam distribution. The difficulty in its evaluation is usually the background noise and possible beam halo that might be insignificant for the beam use but affects the rms size calculation significantly due to its wide distribution. Usual tricks of the trade for coping with such situations include thresholding (nullification of measurement points with an intensity of less than a few percents of the maximum intensity, for example) and/or fitting of a Gaussian to the measured distribution. However, in many cases, especially at ion source relevant energies, the beam distributions are far from Gaussian in shape, and therefore, the use of a single number for describing the beam size may not be purposeful.

V. PHASE SPACE DISTRIBUTION

The beam quality, often characterized with transverse emittance, is usually the next figure of merit mentioned for ion sources after beam intensity and energy. The importance of beam quality arises from the fact that the beam intensity in itself is not of any value unless the beam can be transported to its intended application, and for optimizing the transport, the phase space distribution of the beam should be known. While it may be possible in simulations used for studying the beam transport to define the full six dimensional phase space (x, p_x, y, p_y, z, p_z) distribution of the beam, measuring all six degrees of freedom at once is very challenging. Therefore, most often, the 2D projectional transverse phase space distributions (x, p_x) and (y, p_y) or 4d distribution (x, p_x, y, p_y) is measured on a plane of constant z. Typically, in such measurements, the longitudinal momentum p_z (or the total momentum p_0) is assumed to be constant, allowing the transverse momenta to be calculated from the trajectory angle $\theta = \arctan p_x/p_z$ or divergence $x' = p_x/p_z$. Thus, the convention is that the transverse phase space distributions are represented in trace spaces (x, x'), (y, y'), and (x, x', y, y'), where the divergences are appended with a unit rad even if they are angles only in the small-angle limit.

The 2D projectional transverse phase space measurements are mostly based on using a movable collimating slit to select a slice of the beam at x (or similarly y) for further analysis. The divergence distribution within the selected slice can then be resolved using a selection of techniques. The first class of systems take advantage of the fact that divergence x' of a particle produces a displacement $\Delta x = x'L$ on a drift length L. The divergence distribution can therefore be scanned either with another movable slit or an SEM wire parallel to the first slit screen at a distance L away in the z-direction. The 2D scanning then provides the distribution of beam current $I(x, x')$ in the phase space. Typically such slit–slit or slit–wire emittance meters are quite slow as they require physical scanning through a 2D grid

of points and are therefore not often used. A way to make such a scanner faster is to replace the second wire with a grid of wires, allowing the device to produce several divergence points simultaneously. In the development work of CERN's Linac4 H^- ion source, for example, such a slit-grid scanner is used to provide a 3.75 mrad divergence resolution and a span of ±86 mrad in one beam pulse by using a 47 wire grid with a 0.75 mm spacing, 200 mm away from the slit.[35,39] The resolution can be doubled by moving the grid by half the wire spacing between two pulses and thus spending double the time for the scan. The scan speed gained with a grid system compared to a single wire or slit is very significant as the Linac4 ion source is operated only with a 1 Hz repetition rate. In addition, by storing the recorded beam current on each grid wire as a function of time, it is possible to analyze the evolution of the beam phase space within the pulse, thus providing essential information on the plasma startup transients and the applicability of the beam for transport at different times. Another example of a fast emittance measurement is from the J-PARC 2 MHz H^- RF ion source, where a slit–slit scanner was used to resolve variations in the beam in the RF excitation timescale, giving insight into the plasma heating and beam formation processes.[40]

Another method for resolving the beam divergence distribution is to use electrostatic bending with parallel plates, as shown in Fig. 4. The transverse electric field between the plates bends the beam slice and selects a divergence going through a second slit into an FC with electron suppression. The divergence selected is $x' = L_{\text{eff}} \frac{V}{2Ud}$, where L_{eff} is the effective plate length, d is the distance between the plates, $\pm V$ are the plate voltages, and U is the source potential. Such a configuration is known as the Allison scanner,[41,42] and it provides fast phase space scanning especially with continuous beams as scanning the plate voltage is much faster than physical scanning of a slit–slit or a slit–wire system.

Another possibility for resolving the divergence is to have a scintillation screen or an MCP plate[43] follow the slit or even have several slits on a single slit plate to sample several slices of the beam at once. Such a system, of course, has to be designed to avoid overlapping of the distributions on the screen. Similarly, instead of a slit plate, it is possible to use a grid of small apertures for sampling the beam in both x and y simultaneously, as shown in Fig. 5. The beamlets passing through the holes then diverge while propagating to the imaging screen and produce a 2D pattern, from which divergence

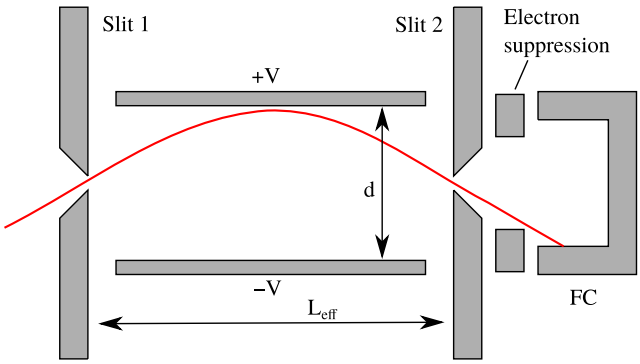

FIG. 4. Allison scanner with a single beamlet passing through to the FC.

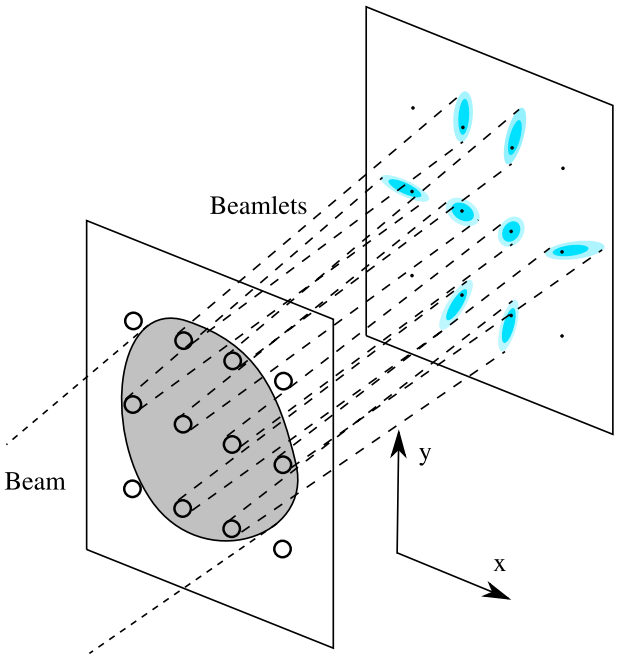

FIG. 5. Pepperpot phase space measurement.

distribution in the (x', y') plane at each aperture location can be extracted. Such a system, typically known as a pepperpot emittance meter,[44] provides a full four dimensional transverse phase space distribution with all cross-correlations such as (x, y'), (x', y'), etc., which cannot be resolved with slit-based phase space measurements. The pepperpot method also has the advantage that the measurement happens at once, while with other scanning methods, the accuracy of the scan is highly dependent on the beam stability. This is not, however, always the case as it is possible to build pepperpot systems with a row of apertures with an advantage of providing an adjustable spatial resolution by means of scanning.[44] With longer phase space scans, it is customary to verify the stability of the ion source by observing the beam intensity with a BCT, for example.

The longitudinal velocity distribution of the extracted ion beam is often probed independently from the transverse distributions by using a so-called retarding field (energy) analyzer (RFEA or RFA). After collimation of the incoming beam in an RFA, the beam is slowed down by a conducting grid with an adjustable potential $U + \Delta U$, where U is typically the ion source plasma chamber potential. Behind the grid, there is a collector connected to an ammeter for recording the ion beam passing through the RFA as a function of the voltage ΔU. Additional grids may be used to provide electron suppression both at the entrance and at the collector.[45] With such a device, the longitudinal energy distribution of the ion beam and the exact source potential, i.e., plasma potential, can be measured.[46–48] The usual way has been to construct the six dimensional particle distribution for modeling purposes from partial data, especially without correlation between the longitudinal and the transverse directions. However, it has been recently demonstrated by Cathey *et al.* with a pulsed H^- beam at 2.5 MeV that a straightforward but slow method of scanning the full six dimensional distribution is applicable and

may reveal previously unknown correlations.[49,50] The method uses a set of slits for choosing a small beamlet at (x, y), and after a drift, there is another set of slits for choosing the divergence (x', y'). The selected beamlet then propagates though a bending magnet, providing the energy resolution, and by timing the beam intensity with respect to the pulse reference, a full 6d distribution is resolved. The method is understandably slow and cumbersome: The first scan took 32 h and produced over $5 \cdot 10^6$ data points. Nevertheless, the equipment required for the measurement is relatively simple, and similar measurements could be carried out in most laboratories if needed.

In most cases, an important part of the phase space measurement is the data analysis and the removal of unidealities such as background noise, ghost images, and amplifier bias. Several studies on this subject have been made with different recommendations for data processing,[51–53] and even if the details vary, the basic recipe is the same. In here, an example of such a process is described for a 2D phase space measurement using an artificially generated dataset of 100×100 pixels with a bi-Gaussian phase space distribution with emittance $\varepsilon_{\mathrm{rms}} = 100$ mm mrad, Gaussian noise with an rms amplitude of 1% of the peak beam signal, and a bias of 0.5%. First, the background data should be analyzed. This is carried out by making a histogram of the pixel values [see Fig. 6(a)] and fitting a Gaussian to the background. The dominant peak should be the background as in a typical scan, the beam occupies a minor phase space area of the whole scan area. This results in the signal bias I_{ave} and the noise standard deviation σ. The data can then be unbiased by subtracting I_{ave} from every pixel after which a threshold level can be defined in multiples of the noise σ. All pixels with signal less than the threshold level are set to zero to remove the background noise. In Fig. 6(b), the thresholded phase space distribution is shown with the 4-rms ellipse $\gamma x^2 + 2\alpha x x' + \beta x'^2 = 4\varepsilon_{\mathrm{rms}}$ calculated from the first and second moments of the data thresholded at 2.5σ using well-known equations for the rms-quantities presented in several papers, such as, for example, Ref. 56. The same calculation can be carried out as a function of the threshold level as presented in Fig. 6(c). In the plot, the increase in computed emittance is observed as the threshold level decreases to below 2.5σ due to the contribution of the noise. The emittance decreases linearly as the thresholding removes parts of the distribution. By using a linear fit in this region and an extrapolation to zero threshold, an estimate on the noise-free emittance value can be produced. The extrapolated value is 96.5 mm mrad in this case, a value quite close to the 100 mm mrad of the distribution. Similarly, extrapolated values for the Twiss parameters α, β, and γ could be produced, but often values simply calculated using a suitable thresholding value, such as 2.5σ in this case, are used. Nevertheless, one should never blindly use emittance values calculated by such data processing without eyeing the plots. The author has found it useful to view the plots presented in Fig. 6 and a black-and-white mask version of Fig. 6(b) identifying the non-zero pixels to avoid contributions even from very weak looking ghost signals. Such ghost signals may have a strong contribution to the emittance value if they are far away from the main distribution and may require manual removal or the use of cluster analysis[53] for automation.

While the use of rms-emittance and Twiss parameters are recommended for characterizing the quality of an ion beam with a stated intensity, these values alone do not fully describe the suitability of the beam for a certain application. The real phase space distributions have non-elliptical shapes [see Fig. 7(b), for example], and the beam density distribution varies (as demonstrated by the typically used Kapchinskij–Vladimirskij, bi-Gaussian, and waterbag phase space distribution models[54]). In many cases, the application has a phase space acceptance within which the beam can be accelerated or transported onward. Therefore, often the plots and numbers presented above are accompanied by an analysis presenting the maximum fraction of the measured ion beam, which can fit inside a hypothetical elliptical acceptance with a given product of half axes. Such an analysis can be made either by keeping the acceptance ellipse shape (orientation and aspect ratio) fixed and just scaling the size or by optimizing the ellipse shape to find the largest fraction for each ellipse size separately.[55] The latter method is more recommended as it corresponds better to the practical case where the beam is tuned by focusing elements to match the acceptance of the following accelerator or transport line (see Fig. 7). Even though often done, such analysis only provides a simplified picture of the system. In most applications, the final applicability of a beam produced should be evaluated with simulations covering the whole beam transport line,

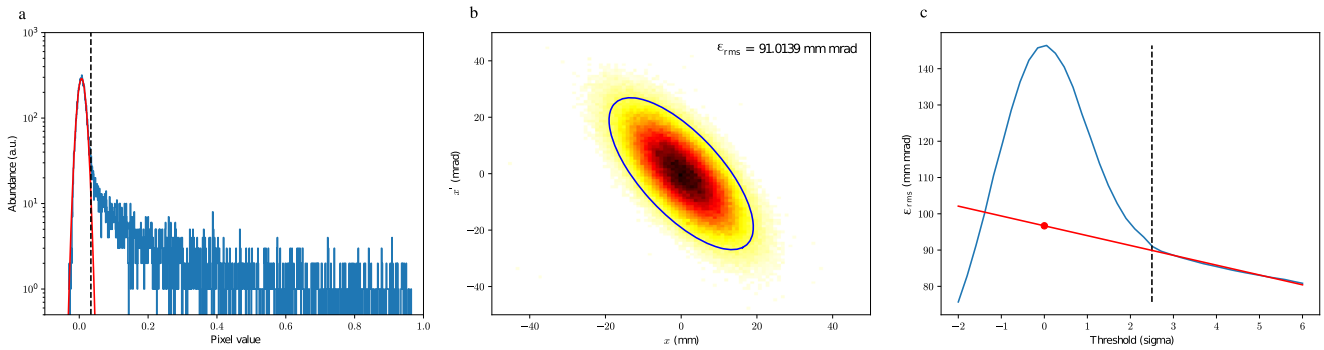

FIG. 6. Example of emittance calculation using artificial data. In (a), a histogram of pixel levels is presented, with a Gaussian fit to the background noise presented in red and a selected threshold level of 2.5σ marked with a dashed line. In (b), the phase space distribution filtered at 2.5σ is shown with the 4-rms ellipse. In (c), the rms-emittance value as a function of threshold level is presented with an extrapolation to zero threshold. It can be seen that the noise starts contributing significantly to the value at threshold levels below 2.5σ, which is marked with the dashed line.

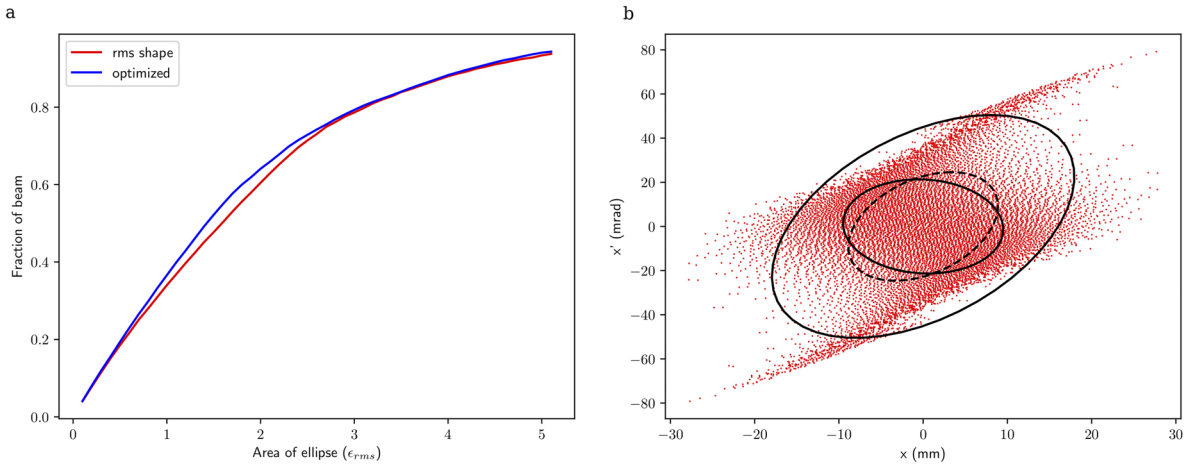

FIG. 7. Example of beam fraction contained within an elliptical acceptance using particle data from an extraction simulation. On the left (a), the red curve shows the fraction with the ellipse shape being fixed to the rms shape, and the blue curve with an optimized shape. On the right (b), the particle distribution and the optimized ellipses with half-axis products ε_{rms} and $4\varepsilon_{rms}$ are shown with a solid line and the rms-ellipse with a dashed line.

taking into account the aberrations, and by using the real non-elliptical acceptance of the application, which in many cases is a function of the beam current due to space-charge forces.

The phase space scan is a critically important diagnostic tool not only because it provides the distribution of the beam to be used for designing the beam transport downstream of the scan location but also for studying the beam formation of the ion source either by backtracking the beam toward the ion source[57] or by comparing beam phase space distributions from simulations to measurements, for example. In the field of ECR ion sources, thorough characterizations of the beams produced have been made with emittance measurements of magnetically separated charge states by Leitner *et al.*[22,58] The measurements and their comparison to the conventionally used model, predicting that emittance increases for each element when charge state increases, indicate that the model does not take into account all the relevant physics. Also here, the backtracking of the 4D phase space could provide direct information on the conditions at the beam formation region, especially the spatial distribution of each charge state at the extraction aperture and the transverse velocity distribution, and therefore, it can provide insight into the ion temperatures and distributions in the ECR plasma. With H^- beam extraction systems, the emittance values have also been used to evaluate the beam formation and its modeling. Systematic emittance measurements made as a function of ion beam intensity varied by adjusting the source plasma density have been shown to act as a probe, which can be used to tune the boundary conditions at the plasma sheath for achieving good predicting power for the extraction modeling tools.[59]

VI. SUMMARY

An overview of the most common ion beam diagnostic techniques used at ion sources is given in this paper. All of these technologies are based on measurement of all or a part of the extracted ion beam. The gauging of the beam current is typically carried out by direct measurement of charges using a Faraday cup, measurement of fields induced by the beam, particle counting, or calorimetry. These technologies are used by themselves for probing the total beam current produced or together with electromagnetic separators to analyze beam mass and charge spectra. By further adding spatial resolution via collimation, beam profiles and phase space distributions can be scanned.

AUTHOR DECLARATIONS

Conflict of Interest

The author has no conflicts to disclose.

DATA AVAILABILITY

The data that support the findings of this study are available from the corresponding author upon reasonable request.

REFERENCES

[1]H. Schmickler, Proceedings of the CERN Accelerator School on Beam Instrumentation, Tuusula, Finland, 2–15 June 2018, https://cas.web.cern.ch/previous-schools.
[2]P. Forck, *Lecture Notes on Beam Instrumentation and Diagnostics* (Joint University Accelerator School, January–March 2017).
[3]H. Winter, F. Aumayr, and G. Lakits, Nucl. Instrum. Methods Phys. Res., Sect. B **58**, 301–308 (1991).
[4]E. J. Sternglass, Phys. Rev. **108**, 1 (1957).
[5]D. Hasselkamp, H. Rothard, K. O. Groeneveld, J. Kemmler, P. Varga, and W. Hannspeter, *Particle Induced Electron Emission II* (Springer-Verlag Berlin Heidelberg, 1992).
[6]T. Schenkel, A. V. Barnes, M. A. Briere, A. Hamza, A. Schach von Wittenau, and D. H. Schneider, Nucl. Instrum. Methods Phys. Res., Sect. B **125**, 153–158 (1997).
[7]Y. Amdidouche, M. Bourgeois, J. L. Collier, and T. R. Sherwood, Nucl. Instrum. Methods Phys. Res., Sect. B **89**, 424–427 (1994).
[8]I. Bojko, N. Hilleret, and C. Scheuerlein, J. Vac. Sci. Technol. A **18**, 972 (2000).

[9]T. Kalvas, O. Tarvainen, T. Ropponen, O. Steczkiewicz, J. Ärje, and H. Clark, Rev. Sci. Instrum. **81**, 02B703 (2010).
[10]E. D. Cantero, A. Sosa, W. Andreazza, E. Bravin, D. Lanaia, D. Voulot, and C. P. Welsch, Nucl. Instrum. Methods Phys. Res., Sect. A **807**, 86–93 (2016).
[11]J. Harasimowicz, C. P. Welsch, L. Cosentino, A. Pappalardo, and P. Finocchiaro, Phys. Rev. Spec. Top.–Accel. Beams **15**, 122801 (2012).
[12]V. Damideh, J. Ali, S. H. Saw, R. S. Rawat, P. Lee, K. T. Chaudhary, Z. H. Rizvi, S. Dabagh, F. D. Ismail, and L. Sing, Phys. Plasmas **24**, 063302 (2017).
[13]R. Geller, *Electron Cyclotron Resonance Ion Sources and ECR Plasmas* (CRC Press, 1996).
[14]R. C. Webber, AIP Conf. Proc. **546**, 83 (2000).
[15]J. B. Sharp, "The induction type beam monitor for the PS: Hereward transformer," Report No. CERN MPS-Int-CO-62-15, 1962.
[16]K. Unser, IEEE Trans. Nucl. Sci. **16**, 934–938 (1969).
[17]K. Unser, AIP Conf. Proc. **252**, 266 (1992).
[18]J. L. Wiza, Nucl. Instrum. Methods **162**, 587–601 (1979).
[19]D. A. Fink, T. Kalvas, J. Lettry, Ø. Midttun, and D. Noll, Nucl. Instrum. Methods Phys. Res., Sect. A **904**, 179–187 (2018).
[20]T. Kalvas, R. F. Welton, O. Tarvainen, B. X. Han, and M. P. Stockli, Rev. Sci. Instrum. **83**, 02A705 (2012).
[21]A. George, T. Kalvas, S. Melanson, N. Savard, D. Potkins, M. Dehnel, and N. G. R. Broderick, Rev. Sci. Instrum. **91**, 013306 (2020).
[22]D. Leitner, D. Winklehner, and M. Strohmeier, J. Instrum. **6**, P07010 (2011).
[23]I. Izotov, O. Tarvainen, V. Skalyga, D. Mansfeld, T. Kalvas, H. Koivisto, and R. Kronholm, Plasma Sources Sci. Technol. **27**, 025012 (2018).
[24]T. Kalvas, A. Javanainen, H. Kettunen, H. Koivisto, O. Tarvainen, and A. Virtanen, Nucl. Instrum. Methods Phys. Res., Sect. B **406**, 205–209 (2017).
[25]E. Plies, K. Marianowski, and T. Ohnweiler, Nucl. Instrum. Methods Phys. Res., Sect. A **645**, 7–11 (2011).
[26]O. D. Cortázar, A. Megía-Macías, O. Tarvainen, T. Kalvas, and H. Koivisto, Rev. Sci. Instrum. **86**, 083309 (2015).
[27]L. Chen, X. Wan, D. Z. Jin, X. H. Tan, Z. X. Huang, and G. B. Tan, Rev. Sci. Instrum. **86**, 035107 (2015).
[28]M. Vogel, D. F. A. Winters, H. Ernst, H. Zimmermann, and O. Kester, Nucl. Instrum. Methods Phys. Res., Sect. B **263**, 518–522 (2007).
[29]D. Jiménez-Rey, B. Zurro, G. García, A. Baciero, L. Rodríguez-Barquero, and M. García-Munoz, J. Appl. Phys. **104**, 064911 (2008).
[30]T. Nagatomo, V. Tzoganis, M. Kase, O. Kamigaito, and T. Nakagawa, Rev. Sci. Instrum. **87**, 02B920 (2016).
[31]D. S. Todd, D. Leitner, and M. M. Strohmeier, in *Proceedings of the 13th Beam Instrumentation Workshop* (Lawrence Berkeley National Laboratory, Tahoe City, California, USA, 4–8 May 2008), pp. 227–231.
[32]R. Nocentini, F. Bonomo, A. Pimazzoni, U. Fantz, P. Franzen, M. Fröschle, B. Heinemann, R. Pasqualotto, R. Riedl, B. Ruf, and D. Wünderlich, AIP Conf. Proc. **1655**, 060006 (2015).
[33]D. Knolle, D. Ratschko, and M. Gläser, Rev. Sci. Instrum. **67**, 3082 (1996).
[34]L. Panitzsch, M. Stalder, and R. F. Wimmer-Schweingruber, Rev. Sci. Instrum. **80**, 113302 (2009).
[35]F. Roncarolo, U. Raich, and F. Zocca, in *Proceedings of the 27th International Linear Accelerator Conference* (CERN, Geneva, Switzerland, 31 August–5 September 2014), pp. 502–505.
[36]A. Beller, D. Bondoux, and F. Bouly, in *Proceedings of the 10th International Particle Accelerator Conference* (Australian Nuclear Science and Technology Organisation, Melbourne, Australia, 19–24 May 2019), pp. 2466–2469.
[37]M. Auger, S. Braccini, T. S. Carzaniga, A. Ereditato, K. P. Nesteruk, and P. Scampoli, J. Instrum. **11**, P03027 (2016).
[38]F. Becker, in *Proceedings of the 10th European Workshop on Beam Diagnostics and Instrumentation for Particle Accelerators* (Deutsches Elektronen Synchrotron, Hamburg, Germany, 16–18 May 2011), pp. 575–578.
[39]J. Lettry, D. Aguglia, S. Bertolo, S. Briefi, A. Butterworth, Y. Coutron, A. Dallocchio, N. David, E. Chaudet, U. Fantz *et al.*, AIP Conf. Proc. **1869**, 030002 (2017).
[40]T. Shibata, K. Shinto, M. Wada, H. Oguri, K. Ikegami, K. Ohkoshi, and K. Nanmo, AIP Conf. Proc. **2373**, 050002 (2021).
[41]P. W. Allison, J. D. Sherman, and D. B. Holtkamp, IEEE Trans. Nucl. Sci. **30**, 2204–2206 (1983).
[42]M. P. Stockli, R. F. Welton, R. Keller, and M. Leitner, Rev. Sci. Instrum. **77**, 03B706 (2006).
[43]S. Kondrashev, A. Barcikowski, A. Levand, P. N. Ostroumov, R. C. Pardo, G. Savard, R. H. Scott, T. Sun, R. C. Vondrasek, and G. P. Zinkannet, in *Proceedings of the 25th Linear Accelerator Conference* (JACOW, Tsukuba, Japan, September 12–17 2010), pp. 608–610.
[44]H. R. Kremers, J. P. M. Beijers, and S. Brandenburg, Rev. Sci. Instrum. **84**, 025117 (2013).
[45]T. H. M. van de Ven, C. A. de Meijere, R. M. van der Horst, M. van Kampen, V. Y. Banine, and J. Beckers, Rev. Sci. Instrum. **89**, 043501 (2018).
[46]M. Sarstedt, P. Herz, W. B. Kunkel, Y. Lee, K. N. Leung, L. Perkins, D. Pickard, M. Weber, M. D. Williams, and E. Hammel, in *Proceedings of the 16th Particle Accelerator Conference* (The American Physical Society, Dallas, TX, USA, 1–5 May 1995), pp. 2542–2544.
[47]O. Tarvainen, P. Suominen, and H. Koivisto, Rev. Sci. Instrum. **75**, 3138 (2004).
[48]O. Tarvainen, H. Koivisto, T. Ropponen, V. Toivanen, Y. Higurashi, and T. Nakagawa, in *Proceedings of the 19th International Workshop on ECRIS* (Grenoble, France, 23–26 August 2010), pp. 93–95.
[49]B. Cathey, A. Aleksandrov, S. Cousineau, and A. Zhukov, in *Proceedings of the 9th International Particle Accelerator Conference* (TRIUMF, Vancouver, BC, Canada, April 29–May 4 2018), pp. 1107–1109.
[50]B. Cathey, S. Cousineau, A. Aleksandrov, and A. Zhukovet, Phys. Rev. Lett. **121**, 064804 (2018).
[51]M. Stockli, R. F. Welton, R. Keller, A. P. Letchford, R. W. Thomae, and J. W. G. Thomasonet, AIP Conf. Proc. **639**, 135 (2002).
[52]B. Bazak and L. Weissman, J. Instrum. **3**, T02001 (2008).
[53]G. Hahn, T.-K. Yang, H. J. You, and J.-G. Hwang, IEEE Trans. Instrum. Meas. **70**, 1–7 (2021).
[54]T. Kalvas, "Beam extraction and transport," in *Proceedings of CERN Accelerator School on Ion Sources* (CERN, Senec, Slovakia, 29 May–8 June 2012), pp. 537–564, arXiv:1401.3951.
[55]R. Keller, J. D. Sherman, and P. Allison, IEEE Trans. Nucl. Sci. **32**, 2579 (1985).
[56]M. Zhang, "Emittance formula for slits and pepper-pot measurement," Fermi National Accelerator Laboratory, Report No. FNAL-TM-1988, 1996.
[57]D. Noll, V. Bencini, J. B. Lallement, J. Lettry, A. M. Lombardi, F. Di Lorenzo, S. Mattei, and M. O'Neil, AIP Conf. Proc. **2011**, 080026 (2018).
[58]D. Winklehner, D. Leitner, J. Y. Benitez, C. M. Lyneis, and M. M. Strohmeier, Rev. Sci. Instrum. **83**, 02B706 (2012).
[59]T. Kalvas and J. Lettry, AIP Conf. Proc. **2052**, 050007 (2018).